Check for updates

Received: 1 March 2020 | Revised: 30 July 2020 | Accepted: 29 August 2020

DOI: 10.1002/rnc.5238

SPECIAL ISSUE ARTICLE

WILEY

Event-triggered distributed model predictive control for resilient voltage control of an islanded microgrid

Pudong Ge[1] | **Boli Chen**[2] | **Fei Teng**[1]

[1]Department of Electrical and Electronic Engineering, Imperial College London, London, UK

[2]Department of Electronic and Electrical Engineering, University College London, London, UK

Correspondence
Fei Teng, Department of Electrical and Electronic Engineering, Imperial College London, London SW7 2AZ, UK.
Email: f.teng@imperial.ac.uk

Funding information
EPSRC, Grant/Award Number: EP/T021780/1; ESRC, Grant/Award Number: ES/T000112/1

Summary

This article addresses the problem of distributed secondary voltage control of an islanded microgrid (MG) from a cyber-physical perspective. An event-triggered distributed model predictive control (DMPC) scheme is designed to regulate the voltage magnitude of each distributed generators (DGs) in order to achieve a better trade-off between the control performance and communication and computation burdens. By using two novel event triggering conditions that can be easily embedded into the DMPC for the application of MG control, the computation and communication burdens are significantly reduced with negligible compromise of control performance. In addition, to reduce the sensor cost and to eliminate the negative effects of nonlinearity, an adaptive nonasymptotic observer is utilized to estimate the internal and output signals of each DG. Thanks to the deadbeat observation property, the observer can be applied periodically to cooperate with the DMPC-based voltage regulator. Finally, the effectiveness of the proposed control method has been tested on a simple configuration with four DGs and the modified IEEE-13 test system through several representative scenarios.

KEYWORDS

distributed model predictive control, event-triggered control, microgrid, nonasymptotic observer, resilience

1 | INTRODUCTION

A microgrid (MG) is a single controllable entity with interconnected loads and distributed energy resources.[1-3] Combining these physical plants with indispensable measurement and control loops, MG has been investigated as a typical cyber-physical system (CPS).[4] A MG can connect and disconnect from the grid to operate in either grid-connected or islanded mode.[1,5] When in the islanded mode, MG control architecture can be divided into three parts: primary control, secondary control, and tertiary control.[6,7] The primary control is implemented locally, whereas the secondary and tertiary control coordinate the controllable distributed generators (DGs) in the MG to achieve respective control objectives: commonly the objective of the secondary control is to regulate the voltage/frequency to its references and to guarantee the accurate power sharing, while the objective of the tertiary control is to achieve the economic dispatch.[2,6,8]

This is an open access article under the terms of the Creative Commons Attribution License, which permits use, distribution and reproduction in any medium, provided the original work is properly cited.
© 2020 The Authors. *International Journal of Robust and Nonlinear Control* published by John Wiley & Sons Ltd.

This article focuses on the secondary control of the MGs. Initial research on this topic investigates the centralized control strategies,[9] where DGs receive control commands from a center controller. However, due to the fact that the centralized control structure suffers communication delays and requires extensive communication and computation infrastructure, the distributed control strategies, which allow each DG to communicate only with neighboring DGs, have received increasing attention.[10,11] In particular, distributed control strategies such as linear feedback control,[12-14] finite-time control,[15,16] fixed-time control,[17] have been applied to improve the secondary control in the MG with sparse communication network. Model predictive control (MPC)[18] has been recently introduced to distributed MG voltage control and demonstrated its superior performance. However, MPC algorithm exacerbates the burden on the online computation and real-time communication due to its prediction mechanism. Most of the existing distributed secondary control methods of the MG[15,17,19,20] are still designed and implemented in a time-triggered fashion, where the sensoring and the controlling are conducted periodically. The time-triggered control could lead to inefficient utilization of computation and communication resources as many data transmissions and calculations are not actually essential to guarantee the control performance.

In this context, the event-triggered control has been proposed for distributed model predictive control (DMPC) to achieve a better trade-off between the control performance and communication and computation burden.[21-23] The event-triggered mechanism can ease the burden on the communication and even keep resilient against reduced communication resources caused by cyber contingency. So far, several event-triggered secondary control methods have been developed in the MG system with droop-based DGs. However, several problems still remain: (i) the triggering conditions for simultaneously reducing computation and communication have not been fully considered; (ii) the resilience brought by the prediction mechanism of the DMPC to the possible cyber events has not been fully discussed; (iii) the existing event-triggered MG control methods[14,24] are designed with the assumption that the system state information are fully available, which may not be the case for certain system configuration or requires continuously running of an observer.

To mitigate the aforementioned problems, a distributed resilient voltage control of an islanded MG is designed based on an event-triggered DMPC and an adaptive nonasymptotic observer. The main contributions of this article are as follows:

(i) A novel distributed event-triggered DMPC framework is proposed to restore the voltage for islanded MGs. The proposed DMPC algorithm fully considers the dynamics brought by the DG primary control loop, and improves the control performance owing to its constraint-based optimization. The prediction model of the DMPC also can compensate the effect of communication failure to enhance the system resilience by the update principle of the prediction sequence. In addition, two event triggering conditions which can be easily embedded into the DMPC are designed respectively to reduce computation and communication burden in the cyber layer.

(ii) An adaptive nonasymptotic observer is designed to facilitate a cost-effective output-based control framework, which, unlike the Luenberger-like observer,[25,26] can operate in an intermittent way due to its deadbeat convergence property; Moreover, the integrated control framework that coordinates the proposed DMPC voltage regulator and the nonasymptotic observer is designed from a timing sequence perspective.

The remainder of this article is organized as follows. Section 2 is concerned with the cyber-physical modeling of the islanded MG and the corresponding problem formulation. In Section 3, the DMPC with specific event-triggered mechanism and the adaptive nonasymptotic observer are detailed. The corresponding simulation cases are provided in Section 4, and the conclusions are collected in Section 5.

Primary notations and definitions are given as follows. The set of real numbers is denoted by $\mathbb{R}$. For any vector $\boldsymbol{x}$, $\|\boldsymbol{x}\|$ denotes the Euclidean norm and $\|\boldsymbol{x}\|_{\mathbf{Q}} = \sqrt{\boldsymbol{x}^T\mathbf{Q}\boldsymbol{x}}$ stands for $\mathbf{Q}$-weighted norm, where $\mathbf{Q}$ is a matrix with appropriate dimension. The notation $\mathbf{Q} > 0$ denotes that $\mathbf{Q}$ is a positive definite matrix. For any set N, $|N|$ denotes the number of elements in N. For any nth order differentiable $y(t)$, $y^{(n)}(t)$ denotes the nth order differential value. The notation $\mathbf{1}_n \in \mathbb{R}^n$ denotes a column vector with all elements being ones, that is, $\mathbf{1}_n = [1, 1, \ldots, 1]^T$. The notation $\mathbf{I}_n$ denotes the nth order identity matrix.

2 | PROBLEM FORMULATION

In this section, the model for designing distributed control method of an islanded microgrid is detailed from a cyber-physical coupling system perspective. The physical system contains the electrical topology of the MG and its local controllers, while the cyber layer of the MG can be modeled as a multiagent system with interconnecting communications, as shown in Figure 1.

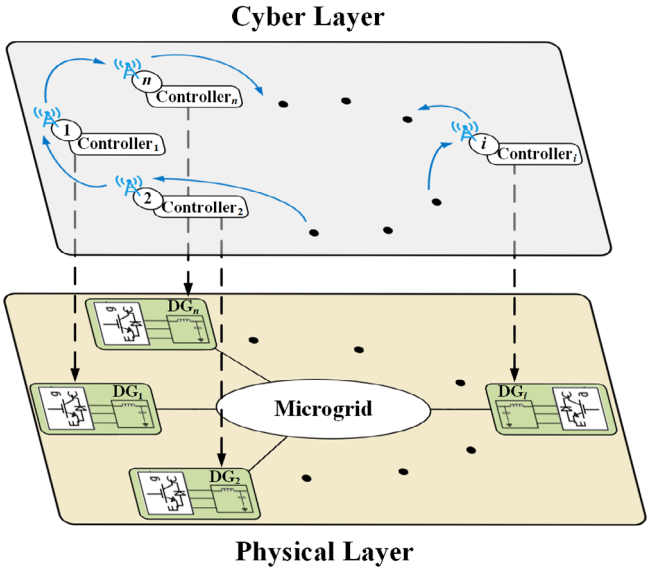

FIGURE 1 Distributed control structure of a cyber-physical coupling MG [Colour figure can be viewed at wileyonlinelibrary.com]

2.1 | Physical system

The MG physically contains multiple DGs that are interconnected through the electrical network. If there is a line between DG i and DG j with the impedance $Z_{ij} = R_{ij} + jX_{ij}$, due to the inductive impedance,[14,27] the output active power and reactive power of DG i can be expressed as follows:

$$P_i = P_{iL} + \sum_{j=1}^{N_i} \frac{V_i V_j}{X_{ij}} \sin(\theta_i - \theta_j), \tag{1}$$

$$Q_i = Q_{iL} + \sum_{j=1}^{N_i} \left[\frac{V_i^2}{X_{ij}} - \frac{V_i V_j}{X_{ij}} \cos(\theta_i - \theta_j) \right], \tag{2}$$

where P_{iL} and Q_{iL} are active and reactive power of the load at bus i; and V_i and θ_i are the bus voltage and the angle at bus i. In practice, the electrical network connecting DG i and DG j is usually more complicated. However, it is reasonable to model each single MG system by using approximate modeling approaches, where the line impedance is modeled as the equivalent impedance of the network.[28,29]

Due to the fact that the phase difference $(\theta_i - \theta_j)$ is small,[30] $\sin(\theta_i - \theta_j) \approx (\theta_i - \theta_j)$ and $\cos(\theta_i - \theta_j) \approx 1$, which means the active and reactive power can be controlled by the difference of phase angle and voltage magnitude, respectively. Thus, the conventional droop control can be obtained:

$$\omega_i = \omega_{ni} - m_{Pi} P_i, \tag{3}$$

$$V_i = v_{odi}^* = V_{ni} - n_{Qi} Q_i, \tag{4}$$

where ω_i, V_i are the angular frequency and the voltage magnitude provided for the inner control loops. m_{Pi}, n_{Qi} are droop coefficients and are selected based on the active and reactive power ratings of each DG.[7] ω_{ni}, V_{ni} are the nominal references of the primary control, which can be generated from the secondary control. It should be noted that each DG is controlled under itself d-q (direct-quadrature) axis, which guarantees the voltage magnitude V_i is equivalent to the d-axis voltage v_{odi}, which means $v_{oqi}^* = 0$. Through the droop control principle, each inverter is controlled with its rotating angular reference. To model the MG in a uniform frame, a specifically chosen DG is considered as the common reference ω_{com}, and the angular frequency difference of the ith DG can be denoted by δ_i:

$$\dot{\delta}_i = \omega_i - \omega_{com}. \tag{5}$$

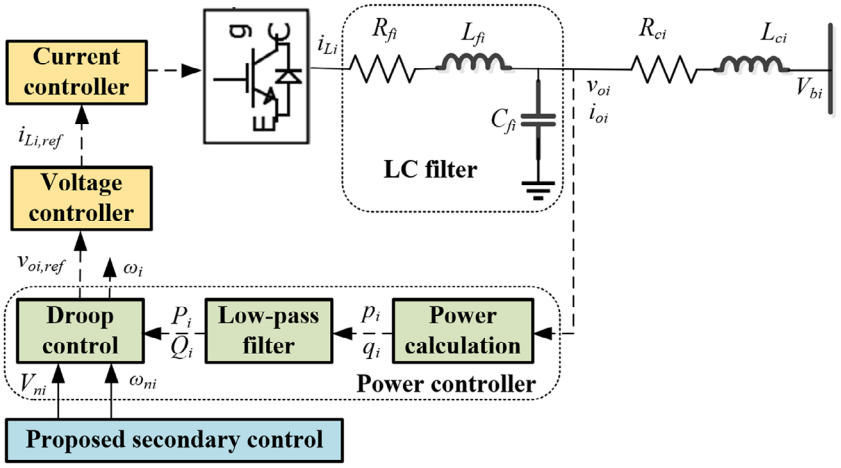

FIGURE 2 Block diagram of the primary control loops in the inverter-based DG [Colour figure can be viewed at wileyonlinelibrary.com]

Combining detailed models in the DG control loops as shown in Figure 2 (including models of inner loops shown in the Appendix), the large-signal dynamic model of the ith DG can be detailed as the following multiinput multioutput (MIMO) nonlinear system:

$$\dot{\boldsymbol{x}}_i = \boldsymbol{f}_i(\boldsymbol{x}_i) + \boldsymbol{g}_i(\boldsymbol{x}_i)\boldsymbol{u}_i + \boldsymbol{k}_i(\boldsymbol{x}_i)\boldsymbol{d}_i(\boldsymbol{x}_j) \tag{6}$$

with the state vector

$$\boldsymbol{x}_i = [\delta_i \; P_i \; Q_i \; \phi_{di} \; \phi_{qi} \; \gamma_{di} \; \gamma_{qi} \; i_{ldi} \; i_{lqi} \; v_{odi} \; v_{oqi} \; i_{odi} \; i_{oqi}]^T,$$

where the system input is denoted by $\boldsymbol{u}_i = [\omega_{ni} \; V_{ni}]^T$ with ω_{ni} and V_{ni} being the input variables for frequency control and voltage control, respectively. $\boldsymbol{d}_i(\boldsymbol{x}_j) = [\omega_{com} \; v_{bdi} \; v_{bqi}]^T$ represents the interconnection with other DGs, modeled as a disturbance in a single DG system, and v_{bdi}, v_{bqi} denote the d-q-axis voltages at the connection bus in Figure 2, which reflects the external disturbance acting on DG i.

2.2 | Cyber system

To realize the implementation of the secondary controllers, we assume each DG is equipped with a transceiver for information exchange among sparsely distributed DGs. Thus, as depicted in Figure 1, the communication network in the multi-DG MG can be modeled as a weighted graph $\mathcal{G}_c = \{\mathcal{V}_c, \mathcal{E}_c\}$, where $\mathcal{V}_c = \{v_1, v_2, \ldots, v_N\}$ is a set of nodes, $\mathcal{E}_c \subseteq \mathcal{V}_c \times \mathcal{V}_c$ is a set of edges, and N is the number of controllable DG nodes. A edge (v_j, v_i) means that the ith node can receive information from the jth node and v_j is a neighbor of v_i. The set of neighbors of node i is described by $N_i = \{j : (v_j, v_i) \in \mathcal{E}_c$. The corresponding adjacency matrix $\mathcal{A} = [a_{ij}] \in \mathbb{R}^{N\times N}$ is denoted by $a_{ii} = 0$; $a_{ij} > 0$ if $(v_j, v_i) \in \mathcal{E}_c$, otherwise $c_{ij} = 0$. For the graph representing a MG, there exists a virtual leader (reference node), whose adjacency matrix is denoted by $\mathcal{B} = \text{diag}\{b_i\} \in \mathbb{R}^{m\times m}$, and the Laplacian matrix $\mathcal{L} = \mathcal{D} - \mathcal{A} + \mathcal{B}$, where $\mathcal{D} = \text{diag}\{\sum_{j\in N_i} a_{ij}\}$.[19,31]

The objective of the secondary voltage control designed in the cyber system is to regulate the output voltage magnitude V_i of each DG to a unified reference v_{ref} through a leader-following scheme, in the sense that $v_{ref,1} = v_{ref}$ and $v_{ref,i} = V_{i-1}, \forall i > 1$. In other words, each DG tracks its neighbors' voltage to achieve the reference tracking. In the cyber layer design, it is meaningful and desirable to limit the computation and communication, especially with the wireless embedded control systems.[21] From this point of view, this article proposes an event-triggered control framework, where, as opposed to the conventional control with continuous (or periodic) observation and control of the system, control tasks are executed only when certain conditions are met in order to minimize the computation and communication costs.

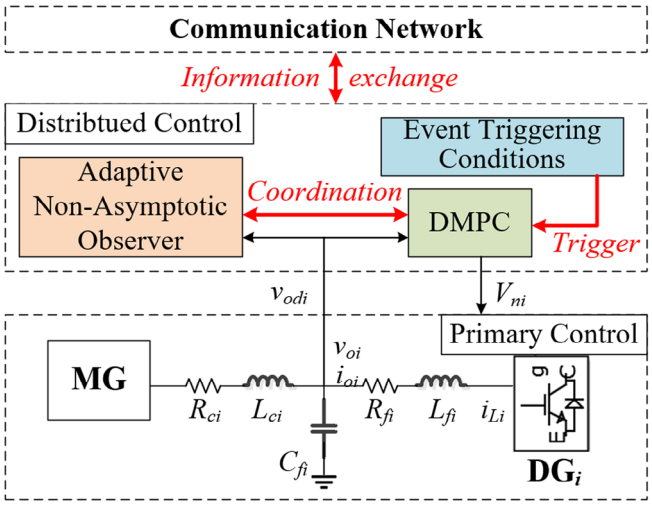

FIGURE 3 Scheme of the DMPC based noise-resilient voltage control [Colour figure can be viewed at wileyonlinelibrary.com]

3 | LINEAR DMPC BASED RESILIENT VOLTAGE CONTROL ALGORITHM DESIGN

The proposed control scheme, as shown in Figure 3, is mainly comprised of three parts: distributed model predictive control (DMPC) based voltage regulator, event triggering mechanism design, and adaptive nonasymptotic observer. The voltage regulator is designed based on the DMPC framework, where the event-triggered mechanism can be easily embedded to alleviate the computation burden. In addition, the information exchange among agents is also governed by the event-triggered scheme in order to reduce communication cost. Finally, to reduce sensor cost, an adaptive nonasymptotic observer is utilized for the reconstruction of internal and output signals. Owing to its fast convergence property, the observer can be operated in an intermittent way, and consequently, it can be integrated into the overall event-triggered control framework.

3.1 | DMPC-based voltage restoration

The system model (6) is a MIMO nonlinear system, but when voltage control is considered, instead of using such a sophisticated model, feedback linearization[12] is utilized to simplify the model into a linearized form:

$$\begin{cases} \dot{y}_{i,1} = \dot{v}_{odi} = y_{i,2} \\ \dot{y}_{i,2} = \ddot{v}_{odi} = f_i(\boldsymbol{x}_i) + g_i u_i \\ y_{i,o} = y_{i,1} = v_{odi} \end{cases}, \tag{7}$$

$$\begin{aligned} f_i(\boldsymbol{x}_i) = L_{\boldsymbol{F}_i}^2 h_i(\boldsymbol{x}_i) = (-\omega_i^2 - \frac{K_{Pci}K_{Pvi}+1}{C_{fi}L_{fi}} - \frac{1}{C_{fi}L_{ci}})v_{odi} - \frac{\omega_b K_{Pci}}{L_{fi}} v_{oqi} + \frac{R_{ci}}{C_{fi}L_{ci}} i_{odi} - \frac{2\omega_i}{C_{fi}} i_{oqi} - \frac{R_{fi}+K_{Pci}}{C_{fi}L_{fi}} i_{ldi} \\ + \frac{2\omega_i - \omega_b}{C_{fi}} i_{lqi} - \frac{K_{Pci}K_{Pvi}n_{Qi}}{C_{fi}L_{fi}} Q_i + \frac{K_{Pci}K_{Ivi}}{C_{fi}L_{fi}} \phi_{di} + \frac{K_{Ici}}{C_{fi}L_{fi}} \gamma_{di} + \frac{1}{C_{fi}L_{ci}} v_{bdi}, \\ g_i = L_{\boldsymbol{g}_i} L_{\boldsymbol{F}_i} h_i(\boldsymbol{x}_i) = \frac{K_{Pci}K_{Pvi}}{C_{fi}L_{fi}}, \end{aligned}$$

where $f_i(\boldsymbol{x}_i)$ represents the system nonlinearity.

Let us define an auxiliary control variable $\xi_i = f_i(\boldsymbol{x}_i) + g_i u_i$, then $u_i = (g_i)^{-1}(\xi_i - f_i(\boldsymbol{x}_i))$ and the dynamic system (7) can be rewritten as

$$\begin{cases} \dot{\boldsymbol{y}}_i = \mathbf{A}\boldsymbol{y}_i + \mathbf{B}\xi_i \\ y_{i,o} = \mathbf{C}\boldsymbol{y}_i \end{cases}, \tag{8}$$

$$\boldsymbol{y}_i = \begin{bmatrix} y_{i,1} \\ y_{i,2} \end{bmatrix}, \quad \mathbf{A} = \begin{bmatrix} 0 & 1 \\ 0 & 0 \end{bmatrix}, \quad \mathbf{B} = \begin{bmatrix} 0 \\ 1 \end{bmatrix}, \quad \mathbf{C} = \begin{bmatrix} 1 & 0 \end{bmatrix}.$$

The distributed voltage regulation problem is to find appropriate input ξ_i to achieve $y_{i,o} \to v_{ref,i}$. To implement DMPC, the discrete-time model of (8) is obtained through Euler discretization:

$$\begin{cases} \boldsymbol{y}_i(k+1) = \mathbf{A}_z \boldsymbol{y}_i(k) + \mathbf{B}_z \xi_i(k) \\ y_{i,o}(k) = \mathbf{C}_z \boldsymbol{y}_i(k) \end{cases}, \tag{9}$$

where $\mathbf{A}_z = \mathbf{I} + \mathbf{A}T_s, \mathbf{B}_z = \mathbf{B}T_s, \mathbf{C}_z = \mathbf{C}$ and T_s denotes the sampling time interval. However, after feedback linearization, the dynamics of the discretized system and the real system inevitably differ. An increase in sampling rate will increase the model accuracy whereas computational efficiency degrades. To balance the model accuracy and the computational complexity, we design a two-time-scale DMPC model where two time intervals T_s, T_s^{mpc} are defined. T_s denotes the discretization time interval, while T_s^{mpc} denotes the sampling time interval of the DMPC algorithm, and $T_s^{mpc} = rT_s, r \in \mathbb{Z}^+$. Define $h = 1, 2, \dots, H$ as the prediction time steps of the DMPC, the full model-based prediction at the time-step k ($t_{k+1} - t_k = T_s^{mpc}$) is expressed as

$$y_{i,o}(k + h_d|k) = \mathbf{C}_z \mathbf{A}_z^{h_d} \boldsymbol{y}_i(k) + \sum_{i=0}^{h_d-1} \mathbf{C}_z \mathbf{A}_z^{h_d-i-1} \mathbf{B}_z \xi_i(k+i|k), \quad h_d = 1, 2, \dots, Hr, \tag{10}$$

where h_d denotes the detailed prediction time steps with length Hr for the discretization model, and the model (10) also can be expressed in a matrix form:

$$\begin{bmatrix} y_{i,o}(k+1|k) \\ y_{i,o}(k+2|k) \\ \dots \\ y_{i,o}(k+Hr|k) \end{bmatrix} = \begin{bmatrix} \mathbf{C}_z \mathbf{A}_z \\ \mathbf{C}_z \mathbf{A}_z^2 \\ \dots \\ \mathbf{C}_z \mathbf{A}_z^{Hr} \end{bmatrix} \boldsymbol{y}_i(k) + \begin{bmatrix} \mathbf{C}_z \mathbf{B}_z & & & \\ \mathbf{C}_z \mathbf{A}_z \mathbf{B}_z & \mathbf{C}_z \mathbf{B}_z & & \\ \vdots & \vdots & \ddots & \\ \mathbf{C}_z \mathbf{A}_z^{Hr-1} \mathbf{B}_z & \mathbf{C}_z \mathbf{A}_z^{Hr-2} \mathbf{B}_z & \dots & \mathbf{C}_z \mathbf{B}_z \end{bmatrix} \begin{bmatrix} \xi_i(k|k) \\ \xi_i(k+1|k) \\ \dots \\ \xi_i(k+Hr-1|k) \end{bmatrix}. \tag{11}$$

However, only the prediction at each DMPC time step $k = r, 2r, \dots$ is required, and therefore the order of the model-based prediction can be reduced and expressed as

$$\begin{aligned} \boldsymbol{Y}_{i,o}(k) = \begin{bmatrix} y_{i,o}(k+r|k) \\ y_{i,o}(k+2r|k) \\ \dots \\ y_{i,o}(k+Hr|k) \end{bmatrix} &= (\mathbf{I}_H \otimes [\mathbf{0}_{1\times(r-1)} \quad 1]) \begin{bmatrix} y_{i,o}(k+1|k) \\ y_{i,o}(k+2|k) \\ \dots \\ y_{i,o}(k+Hr|k) \end{bmatrix} = (\mathbf{I}_H \otimes [\mathbf{0}_{1\times(r-1)} \quad 1]) \begin{bmatrix} \mathbf{C}_z \mathbf{A}_z \\ \mathbf{C}_z \mathbf{A}_z^2 \\ \dots \\ \mathbf{C}_z \mathbf{A}_z^{Hr} \end{bmatrix} \boldsymbol{y}_i(k) \\ &+ (\mathbf{I}_H \otimes [\mathbf{0}_{1\times(r-1)} \quad 1]) \begin{bmatrix} \mathbf{C}_z \mathbf{B}_z & & & \\ \mathbf{C}_z \mathbf{A}_z \mathbf{B}_z & \mathbf{C}_z \mathbf{B}_z & & \\ \vdots & \vdots & \ddots & \\ \mathbf{C}_z \mathbf{A}_z^{Hr-1} \mathbf{B}_z & \mathbf{C}_z \mathbf{A}_z^{Hr-2} \mathbf{B}_z & \dots & \mathbf{C}_z \mathbf{B}_z \end{bmatrix} (\mathbf{I}_H \otimes \mathbf{1}_r) \begin{bmatrix} \xi_i(k|k) \\ \xi_i(k+1|k) \\ \dots \\ \xi_i(k+H-1|k) \end{bmatrix} \\ &= \mathbf{F}_i \boldsymbol{y}_i(k) + \mathbf{G}_i \boldsymbol{\Xi}_i(k), \end{aligned} \tag{12}$$

where $\boldsymbol{Y}_{i,o} \in \mathbb{R}^{H\times 1}, \mathbf{F}_i \in \mathbb{R}^{H\times 2}, \mathbf{G}_i \in \mathbb{R}^{H\times H}$, and $\boldsymbol{\Xi}_i \in \mathbb{R}^{H\times 1}$, and more specifically

$$[\xi_i(k|k) \quad \xi_i(k+1|k) \quad \cdots \quad \xi_i(k+Hr-1|k)]^T = (\mathbf{I}_H \otimes \mathbf{1}_r) \boldsymbol{\Xi}_i(k). \tag{13}$$

This guarantees the dimension of prediction model (12) does not increase, although the full prediction model (11) is applied to ensure the prediction accuracy of discretization model. In other words, the prediction sequence $\boldsymbol{Y}_{i,o}(k)$ can be obtained directly from (12) instead of (11), and this can save the computation for both prediction and optimization. Due to

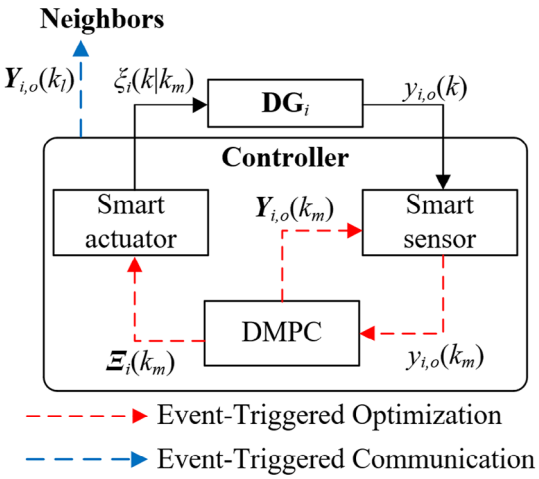

FIGURE 4 Event-triggered DMPC scheme [Colour figure can be viewed at wileyonlinelibrary.com]

the fact that the proposed DMPC tracking voltage reference by eliminating the difference between local and neighboring DGs' voltage magnitudes, the objective function is designed as follows:

$$\min_{\Xi_i(k)} J_i(\mathbf{y}_i(k), \Xi_i(k)) = \left\| \frac{1}{|N_i|} \sum_{j \in N_i} \mathbf{Y}_{i,o}(k) - \mathbf{Y}_{j,o}(k) \right\|_{\mathbf{Q}}^2 + \|\Xi_i(k)\|_{\mathbf{R}}^2, \tag{14}$$

where $|N_i|$ denotes the neighbor number of the ith DG; the weighting matrix $\mathbf{Q} > 0, \mathbf{R} > 0$ are designed to balance the tracking performance and the control effort. It is noteworthy that when solving the optimization problem, the output of the virtual leader (reference node) is a constant vector $\mathbf{Y}_{0,o}(k) = \mathbf{1}_H v_{ref}$. The synchronization of the voltage signals represents the main target of the application addressed in this article. For this reason, the weighting factors $\mathbf{Q}, \mathbf{R}$ are selected to emphasize the former term in (14).

Finally, the DMPC framework is completed by the following constraint

$$0.97 p.u. \leq V_i \leq 1.03 p.u. \tag{15}$$

which restricts the voltage tracking error to 3% so as to enable fast restoration of the voltage to the acceptable range. This constraint can maintain the control performance especially under an exceptional circumstance (eg, a huge voltage drop or an overvoltage). According to IEEE standard 1547, it is not necessary for the power system to strictly fulfill the constraint (15) during the operation. However, the tracking error is not permitted to exceed the 3% limit for more than $\overline{T} = 0.166$ second. In order to meet this requirement, the two sampling interval T_s and T_s^{mpc} calibrated, such that T_s^{mpc} is reasonably smaller than $\overline{T}$ to ensure smooth operation of the system. The optimization problem (14) is solved recursively at each time step k subject to (15), and the first control input $\xi_i(k|k)$ of the optimal control sequence $\Xi_i(k)$ is applied at the ith DG.

3.2 | Event triggering condition design

Traditionally, the DMPC-based voltage regulation algorithm relies on the iterative finite-horizon optimization and information exchange among DGs at each time step k, which heavily increase the computation and communication burdens. In this connection, an event-triggered scheme is designed and integrated into the DMPC framework to effectively save computation and communication power without sacrificing control performance. The overall scheme of a single DG is shown in Figure 4. To better demonstrate the event triggering mechanisms, two sets of samples, are defined: $\mathcal{O} = \{k|\Phi(k)\}$ collects the time steps when the DMPC optimization is triggered, where $\Phi(k)$ and $\Psi(k)$ denote the event-trigger rules for optimization and communication, respectively. The design of these rules is introduced next.

The event-trigger conditions for the DMPC optimization is discussed at first. With the aim of reducing the number of optimization iterations, the DMPC can be made active only when the control performance is not satisfactory. Considering

TABLE 1 Event-triggered voltage regulation algorithm

Event-triggered DMPC iterations in time step k for each DG i	
1:	**given** $k, \boldsymbol{y}_i(k), \boldsymbol{Y}_{j,o}(k), j \in N_i, \boldsymbol{\Xi}_i(k-1)$ (update $\boldsymbol{Y}_{j,o}(k)$ from $\boldsymbol{Y}_{j,o}(k-1)$ as (19) if there is no data received):
2:	**if** (16) holds
3:	solve (14) and (15) to update the control input sequence $\boldsymbol{\Xi}_i(k)$ and the voltage magnitude output sequence $\boldsymbol{Y}_{i,o}(k)$
4:	**else**
5:	update $\boldsymbol{\Xi}_i(k), \boldsymbol{Y}_{i,o}(k)$ according to (17) and (12) respectively
6:	**end if**
7:	apply $\xi_i(k\|k)$ to DG i
8:	**if** (18) holds
9:	transmit $\boldsymbol{Y}_{i,o}(k)$ to the neighbors through the communication network
10:	**end if**

the DMPC is triggered at k_mth step ($k_m \in \mathcal{O}$), then for any $k > k_m$ the DMPC is disabled unless (i) the prediction of the system behavior based on the previously calculated control is not reliable any more, or (ii) the maximum horizon is reached:

$$\Phi(k): \quad \|y_{i,o}(k) - y_{i,o}(k|k_m)\| \geq e_{opt} \qquad \text{OR} \qquad k \geq k_m + H, \tag{16}$$

where $e_{opt} > 0$ is the user designed threshold for the prediction error. By using this event-triggered optimization mechanism (16), the stability proof has been discussed in Reference 22 and the tracking error is bounded. Assuming the DMPC is reactivated at $k_m + n$th step with $1 \leq n \leq H$, the control input is not updated by optimization for any steps in between (ie, $k_m + m, 1 \leq m < n$). Without loss of generality, the input sequence $\boldsymbol{\Xi}_i(k_m + m)$ is updated by

$$\boldsymbol{\Xi}_i(k_m + m) = \begin{bmatrix} \xi_i(k_m + m|k_m) & \cdots & \xi_i(k_m + H - 1|k_m) & 0 \cdots 0 \end{bmatrix}^T, \quad 1 \leq m < n \leq H \tag{17}$$

and based on (17) the output predictions are reevaluated by (12).

On the other hand, to eliminate unnecessary date exchange, the communication between DGs is also regulated by an event-triggered mechanism. Considering the fact that the communication is not required when the consensus among voltage signals of each DG is achieved, after any communication triggered time step k_l, the communication is enabled only when the prediction error meets the following condition:

$$\Psi(k): \quad \|\boldsymbol{Y}_{i,o}(k) - \boldsymbol{Y}_{i,o}(k|k_l)\|_\infty \geq e_{com}, \qquad k > k_l, \tag{18}$$

$$\boldsymbol{Y}_{i,o}(k|k_l) = [[\boldsymbol{Y}_{i,o}(k_l)^T](k - k_l + 1) \quad \cdots \quad [\boldsymbol{Y}_{i,o}(k_l)^T](H) \quad \cdots \quad [\boldsymbol{Y}_{i,o}(k_l)^T](H)]^T, \tag{19}$$

where $[*](i)$ denotes the ith element of the vector. If the communication is not triggered, the neighbors can update the voltage prediction sequence using (19). This can avoid unnecessary communication if a slight change between two consecutive voltage prediction sequences is captured. As such, if the condition (18) is triggered at k_lth time step ($k_l \in C$), the voltage predictions $\boldsymbol{Y}_{i,o}(k_l)$ are updated through the communication network. For any $j \in N_i$, the differences between the voltage of DG i and the information transmitted to DG j in the DMPC algorithm are bounded by the threshold e_{com} for all t.

It should be noted that the voltage prediction remains updated by (19) in presence of communication failure (caused by, e.g., packet loss, denial-of-service) between neighbors as the failure interrupts the communication (i.e., communication is not triggered). In such case, the control terminal value will be the last value in the prediction sequence, which can maintain the performance and enhance the system resilience.

Based on the discussion above, the event-triggered DMPC-based voltage regulation algorithm is illustrated in Table 1. The impacts of the event triggering thresholds e_{opt} and e_{com} on the system behavior will be numerically investigated in Section 4 to provide further insights into the selection of the thresholds.

3.3 | Finite-time adaptive observer design for enhancing noise-resilience

The mismatch between the continuous-time system (8) and the discretized system (9) is highly influenced by the nonlinearity $f_i(\boldsymbol{x}_i)$ embedded in ξ_i due to the variation of f_i within two samples. As such, the evaluation of the $\boldsymbol{y}_i(k+1)$ based on the given control input at $k+1$ may be inaccurate, and in turn, affects the upcoming optimization and prediction. In addition, after generating the auxiliary control variable ξ_i, the actual control input u_i is obtained by $u_i = (g_i)^{-1}(\xi_i - f_i(\boldsymbol{x}_i))$, where the term $f_i(\boldsymbol{x}_i)$ need to be evaluated and additional sensors may be required to monitor the internal states, such as v_{odi}, v_{oqi}. In fact, to obtain the state $\boldsymbol{y}_i$ and the term $f_i(\boldsymbol{x}_i)$, a more cost-effective solution is to use a system observer for reconstructing the real-time state $\boldsymbol{y}_i$ and the time-varying variable $f_i(\boldsymbol{x}_i)$, where the influence of measurement noise can also be highly attenuated.[26] The linearized model (7) considering system disturbance for the ith DG can be rewritten as:

$$\begin{aligned}
&\begin{cases} \dot{y}_{i,1} = y_{i,2} \\ \dot{y}_{i,2} = f_i'(\boldsymbol{x}_i) + g_{i,0}u_i \\ y_{i,o} = y_{i,1} = v_{odi} \end{cases}, \\
&g_i = g_{i,0} + \Delta g_i = L_{\boldsymbol{g}_i} L_{\boldsymbol{F}_i} h_i(\boldsymbol{x}_i), \\
&f_i'(\boldsymbol{x}_i) = f_i(\boldsymbol{x}_i) + \Delta g_i u_i,
\end{aligned} \tag{20}$$

where $[y_{i,1}\ y_{i,2}]^T$ is the original state vector; $g_{i,0}$ and Δg_i denote nominal value and the deviation caused by parameter perturbation of g_i, respectively. Moreover, $f_i'(\boldsymbol{x}_i)$ represents the system uncertainty that collects the dynamics of DG inner control loops $f_i(\boldsymbol{x}_i)$, total uncertainties caused by exogenous disturbance, parameter perturbation, and the measurement noise.

In the sequel, to streamline the notation, let us consider $\boldsymbol{y}_i(t) = \boldsymbol{z}(t) = [z_0(t)\ z_1(t)]^T$ and $y_{i,o}(t) = y(t)$. Then, the single DG system (7) can be rewritten in the following observer-canonical form:

$$\begin{aligned}
&\begin{cases} \dot{\boldsymbol{z}}(t) = \mathbf{A}\boldsymbol{z}(t) + \mathbf{B}u(t) + \mathbf{B}_w w(t) \\ y(t) = \mathbf{C}\boldsymbol{z}(t) \end{cases}, \\
&\mathbf{A} = \begin{bmatrix} a_1 & 1 \\ a_0 & 0 \end{bmatrix}, \quad \mathbf{B} = \begin{bmatrix} b_1 \\ b_0 \end{bmatrix}, \quad \mathbf{C} = \begin{bmatrix} 1 & 0 \end{bmatrix}, \quad \mathbf{B}_w = \begin{bmatrix} \alpha_1 \\ \alpha_0 \end{bmatrix} = \begin{bmatrix} 0 \\ f'(\boldsymbol{x}(t)) \end{bmatrix}, \quad w(t) = 1,
\end{aligned} \tag{21}$$

with $a_0 = a_1 = b_1 = 0, b_0 = 1$.

Motivated by a recently proposed deadbeat adaptive observer,[32] which offers nearly instantaneous convergence property with high noise immunity, the intermittent (over short time-interval) state and parameter estimation can be enabled to cooperate with the proposed DMPC algorithm. Assuming the short time-interval can guarantee that $f'(\boldsymbol{x}(t))$ can be seen as a constant parameter, we can convert the linear time-varying (LTV) system (21) to a linear time-invariant system (LTI) with an unknown parameter $\alpha_0 = f$.

To proceed with the analysis, the state-space system (21) is expressed as the combination of the input-output derivatives:

$$y^{(n)}(t) = \sum_{i=0}^{n-1} a_i y^{(i)}(t) + \sum_{i=0}^{n-1} b_i u^{(i)}(t) + \sum_{i=0}^{n-1} \alpha_i w^{(i)}(t), \tag{22}$$

$$z_r(t) = y^{(r)}(t) - \sum_{j=0}^{r-1} a_{n-r+j} y^{(j)}(t) - \sum_{j=0}^{r-1} b_{n-r+j} u^{(j)}(t) - \sum_{j=0}^{r-1} \alpha_{n-r+j} w^{(j)}(t), \tag{23}$$

where $n = r = 2$ and $\sum_{j=0}^{k}\{\cdot\} = 0, k < 0$. $y^{(n)}(t)$ denotes the nth differential value of $y(t)$ and $z_r(t)$ denotes the rth element of the state in (21).

Let us introduce the Volterra integral operator V_K induced by a bivariate function $K(t,\tau)$ to the output and its derivatives:

$$[V_K y^{(i)}](t) \triangleq \int_0^t K(t,\tau) y^{(i)}(\tau) d\tau, \quad \forall i \in \{0, \dots, n\}, \tag{24}$$

where $K(t,\tau)$ is the nth order nonasymptotic kernel[33] subject to

$$K^{(i)}(t,0)=0,\quad \forall i\in\{0,\ \dots\ ,n\}. \tag{25}$$

After some algebra, we get:

$$[V_K y^{(i)}](t)=\sum_{j=0}^{i-1}(-1)^{i-j-1}y^{(j)}(t)K^{(i-j-1)}(t,t)+(-1)^i[V_{K^{(i)}}y](t), \tag{26}$$

which can be obtained by applying the integral by parts and (25). If $i=1$,

$$[V_{K^{(1)}}y](t)=y(t)K(t,t)-[V_K y^{(1)}](t). \tag{27}$$

Replacing $y(t)$ with $y^{(n-1)}(t)$, (27) becomes

$$[V_{K^{(1)}}y^{(n-1)}](t)=y^{(n-1)}(t)K(t,t)-[V_K y^{(n)}](t),$$

which can be further expanded by substituting (22)

$$\begin{aligned}(-1)^{n-1}[V_{K^{(n)}}y](t)=&-\sum_{j=0}^{n-2}(-1)^{n-2-j}y^{(j)}(t)K^{(n-j-1)}(t,t)+y^{(n-1)}(t)K(t,t)\\&-\sum_{i=0}^{n-1}a_i[V_K y^{(i)}](t)-\sum_{i=0}^{n-1}b_i[V_K u^{(i)}](t)-\sum_{i=0}^{n-1}\alpha_i[V_K w^{(i)}](t).\end{aligned} \tag{28}$$

Substituting (26) and its same forms with $u(t), w(t)$ into (28), we obtain

$$\begin{aligned}&(-1)^{n-1}[V_{K^{(n)}}y](t)+\sum_{i=0}^{n-1}(-1)^i a_i[V_{K^{(i)}}y](t)+\sum_{i=0}^{n-1}(-1)^i b_i[V_{K^{(i)}}u](t)\\&=-\sum_{i=0}^{n-1}(-1)^i\alpha_i([V_{K^{(i)}}w](t)+\sum_{r=0}^{n-1}(-1)^{n-r-1}K^{(n-r-1)}(t,t)z_r(t),\end{aligned} \tag{29}$$

where the state variables $z_r(t)$ and the unknown parameters α_i appear explicitly, and can be obtained by the casual filtering of the signals $y(t), u(t)$.

Considering the specific parameters of (21), the following expression can be inferred from (29):

$$(-1)[V_{K^{(2)}}y](t)+[V_K u](t)=f[V_K w](t)+(-1)K^{(1)}(t,t)z_0(t)+K(t,t)z_1(t). \tag{30}$$

To estimate the state and unknown parameter, let us define

$$\lambda(t)\triangleq(-1)[V_{K^{(2)}}y](t)+[V_K u](t), \tag{31}$$

$$\boldsymbol{\gamma}(t)\triangleq[[V_K w](t),(-1)K^{(1)}(t,t),K(t,t)]. \tag{32}$$

Then, (30) can be rewritten as

$$\lambda(t)=\boldsymbol{\gamma}(t)\begin{bmatrix}f\\ \boldsymbol{z}(t)\end{bmatrix}. \tag{33}$$

To find the estimates of $\begin{bmatrix}f & \boldsymbol{z}(t)\end{bmatrix}^T$ (of dimension 3), we can apply three different nonasymptotic kernel functions to augment (33) into three linearly independent equations

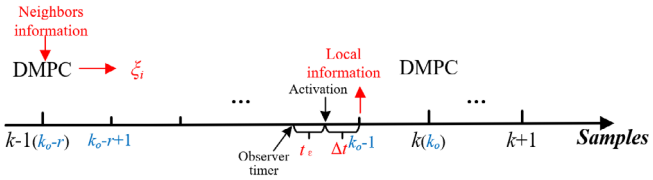

FIGURE 5 Time-sequence cooperation between the event-triggered DMPC and the nonasymptotic observer [Colour figure can be viewed at wileyonlinelibrary.com]

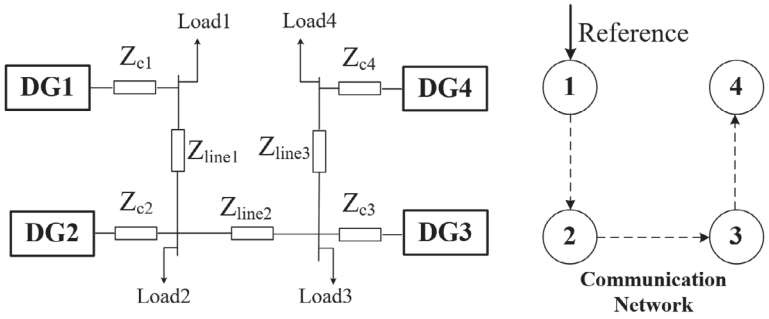

FIGURE 6 Diagram of the tested 4-bus MG system

$$\mathbf{\Lambda}(t) = \mathbf{\Gamma}(t)\begin{bmatrix} f \\ \boldsymbol{z}(t) \end{bmatrix}, \tag{34}$$

where $\mathbf{\Lambda}(t) = [\lambda_0(t), \lambda_1(t), \lambda_2(t)]^T$ and $\mathbf{\Gamma}(t) = [\boldsymbol{\gamma}_0^T(t), \boldsymbol{\gamma}_1^T(t), \boldsymbol{\gamma}_2^T(t)]^T$, and $\lambda_h(t), \boldsymbol{\gamma}_h(t), h \in \{0, 1, 2\}$ are (31) and (32) induced with the kernel functions respectively. The three kernel functions are designed as follows:[33]

$$K_h(t, \tau) = e^{-\omega_h(t-\tau)}(1 - e^{-\varpi\tau})^2, \quad h \in \{0, 1, 2\}, \tag{35}$$

which meets the nonasymptotic condition (25). Finally, the estimates are obtained by:

$$\begin{bmatrix} \hat{f} \\ \hat{\boldsymbol{z}}(t) \end{bmatrix} = \mathbf{\Gamma}^{-1}(t)\mathbf{\Lambda}(t), \quad \forall t_\epsilon < t < t_\epsilon + \Delta t, \tag{36}$$

where t_ϵ is the observer initialization time to guarantee the invertibility of $\mathbf{\Gamma}(t)$ ($\mathbf{\Gamma}(0) = 0$) and Δt is the active time of the observer. The observer ensures finite and instantaneous convergence of the state estimates to the true state with high level of noise immunity. The detailed discussion about the robustness of the observer is show in Reference 34.

The nonasymptotic observer is sampled at T_s and it cooperates with the event-triggered DMPC voltage regulation in a periodical manner, as shown in Figure 5. To ensure the estimates, $\hat{f}_i$ and $\hat{\boldsymbol{y}}_i$, available for the voltage regulator at each DMPC sampling instant. The observer is always enabled $\Delta t + t_\epsilon$ seconds ahead of an MPC step. For example, assuming the time at the kth MPC step is t_{k_o}, the proposed observer is enabled at $t_{k_o} - \Delta t - t_\epsilon$, and after the holding time t_ϵ the estimates start updating. Both estimates $\hat{f}_i(t_{k_o})$ and $\hat{\boldsymbol{y}}_i(t_{k_o})$ are fed to the voltage regulator at t_{k_o} when the observer is disabled.

4 | SIMULATION RESULTS

In this section, the proposed event-triggered control method is tested on a simple MG configuration with four DGs and on the modified IEEE-13 test system.

4.1 | Case 1: 4-DG MG system

The single line diagram of the 4-DG MG and its communication topology is shown in Figure 6. The parameters of the tested MG system and the proposed controllers is shown in Table A1 (see Appendix). The simulation test involves a few representative scenarios by which the effectiveness of the proposed methodology can be reflected.

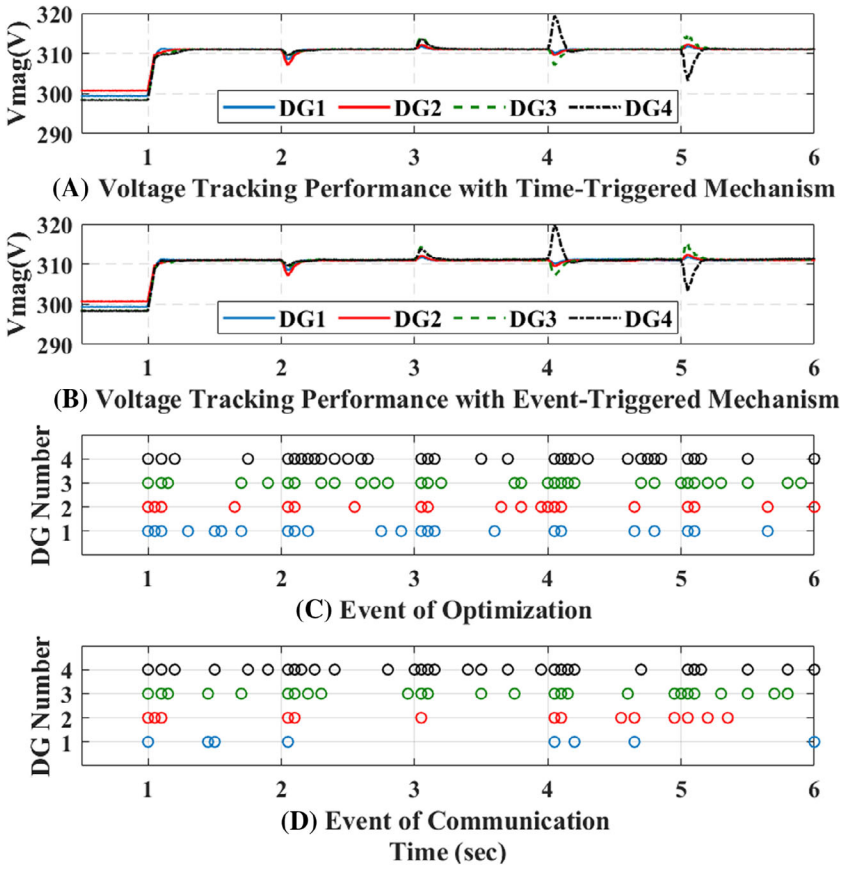

FIGURE 7 Voltage control performance by using event-triggered mechanism: A, voltage tracking performance with time-triggered mechanism; B, voltage tracking performance with event-triggered mechanism; C, event-triggered time of DMPC optimization; D, event-triggered time of neighboring communication [Colour figure can be viewed at wileyonlinelibrary.com]

	DG1	DG2	DG3	DG4	Average
Computation reduction	77%	80%	68%	66%	72.75%
Communication reduction	92%	86%	74%	69%	80.25%

TABLE 2 Computation and communication reductions by using event-triggered mechanism

4.1.1 | Scenario 1: Load change and plug-and-play capability test

In this scenario, the control performance of the proposed control is illustrated under load change and DG's plug-and-play operation: in the beginning, Load2 is disconnect from the system and only primary control is applied; at $t = 1$ second, the proposed secondary control is activated; Load2 and half of Load3 are connected and disconnected at $t = 2$ seconds and $t = 3$ seconds, respectively, and DG4 is disconnected and reconnected at $t = 4$ seconds and $t = 5$ seconds, respectively. The performance of voltage tracking is shown in Figure 7 and the reductions of computation and communication are detailed in Table 2.

By using the event-triggered mechanism, the sacrifice of control performance is limited, whereas the computation and communication are both considerably reduced. By employing the proposed nonasymptotic observer, the negative effects of the disturbance can be eliminated, as shown in Figure 8. The performance of the proposed observer is emphasized by the comparisons among true values, observed values, and disturbance contaminated values that are obtained from indirect measurement in the noisy environment. Compared with the previous Luenberger-like extended state observer,[26] the proposed nonasymptotic observer benefits from its intermittent operating characteristic. The performance comparisons between intermittent operating Luenberger-like observer and the proposed nonasymptotic observer is shown in Figure 9, where we can see that Luenberger-like observer cannot estimate the state precisely when the system responses to the physical events. If the Luenberger-like extended state observer is working intermittently as the proposed nonasymptotic observer, the voltage tracking performance will degrade as Figure 9B.

To further illustrate the resilient performance of the DMPC-based algorithm, an extreme condition with a dramatic voltage drop has been simulated. At $t = 2$ seconds, DG4 is disconnected from the MG while the loads increase, thus the

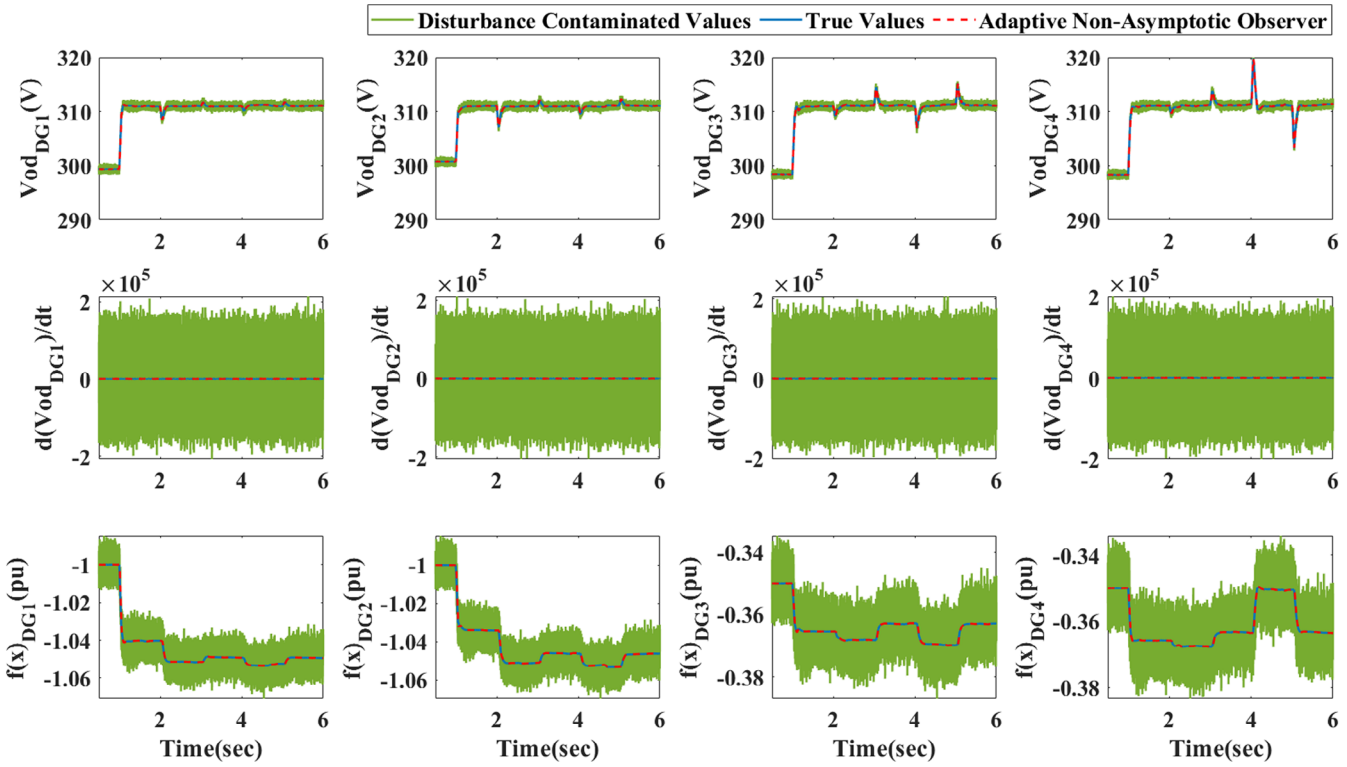

FIGURE 8 Nonasymptotic observer performance (base value of $f(x)$: 7.35×10^9) [Colour figure can be viewed at wileyonlinelibrary.com]

DG output voltage may drop to the unacceptable sections (out of the constraint (15)). Figure 10 compares the control performance between DMPC-based and PI-based algorithms. When using DMPC-based algorithm, the voltage magnitudes are restored into the constraints faster due to the voltage constraints. However, the PI-based algorithm, as a linear control method, cannot handle such a voltage drop efficiently.

4.1.2 | Scenario 2: Control performance with different event triggering thresholds

The control performance of proposed event-triggered mechanism may be influenced by the selection of thresholds for both computation and communication event generators. Therefore, in Scenario 2, case studies as Scenario 1 are carried out with different triggering thresholds.

The control performance with fixed e_{com} ($e_{com} = 0.1$) but different thresholds e_{opt} is detailed in Figure 11 and Table 3. As e_{opt} increases, the optimization computation of each DG controller decreases largely, but from Figure 11, we can also see the control performance will clearly degrade when $e_{opt} = 0.2$ and $e_{opt} = 0.3$. Thus, the selection of e_{opt} is a trade-off between the tracking performance and the computation reduction. The control performance with fixed e_{opt} ($e_{opt} = 0.1$) but different thresholds e_{com} is detailed in Figure 12 and Table 4. As e_{com} increases, the communication among DGs is reduced with the gradually degraded control performance.

4.1.3 | Scenario 3: Effects of information update frequency and prediction horizons

In Scenario 3, the effects of information update frequency and prediction horizon on the control performance are investigated, shown in Figure 13. Figure 13A illustrates the voltage response for different update intervals ($T_s^{mpc} = 0.05, 0.1, 0.15$ seconds). Although the voltage control performance degrades slightly on convergence time as the update interval increases, the computation and communication ($T_s^{mpc} = 0.15$ seconds) are reduced significantly by 32.1% and 68.4% respectively compared with that of $T_s^{mpc} = 0.05$ seconds. The effect of the prediction horizon is shown on the voltage control performance as prediction horizon decreases. It can be noted that the declining prediction horizon leads to

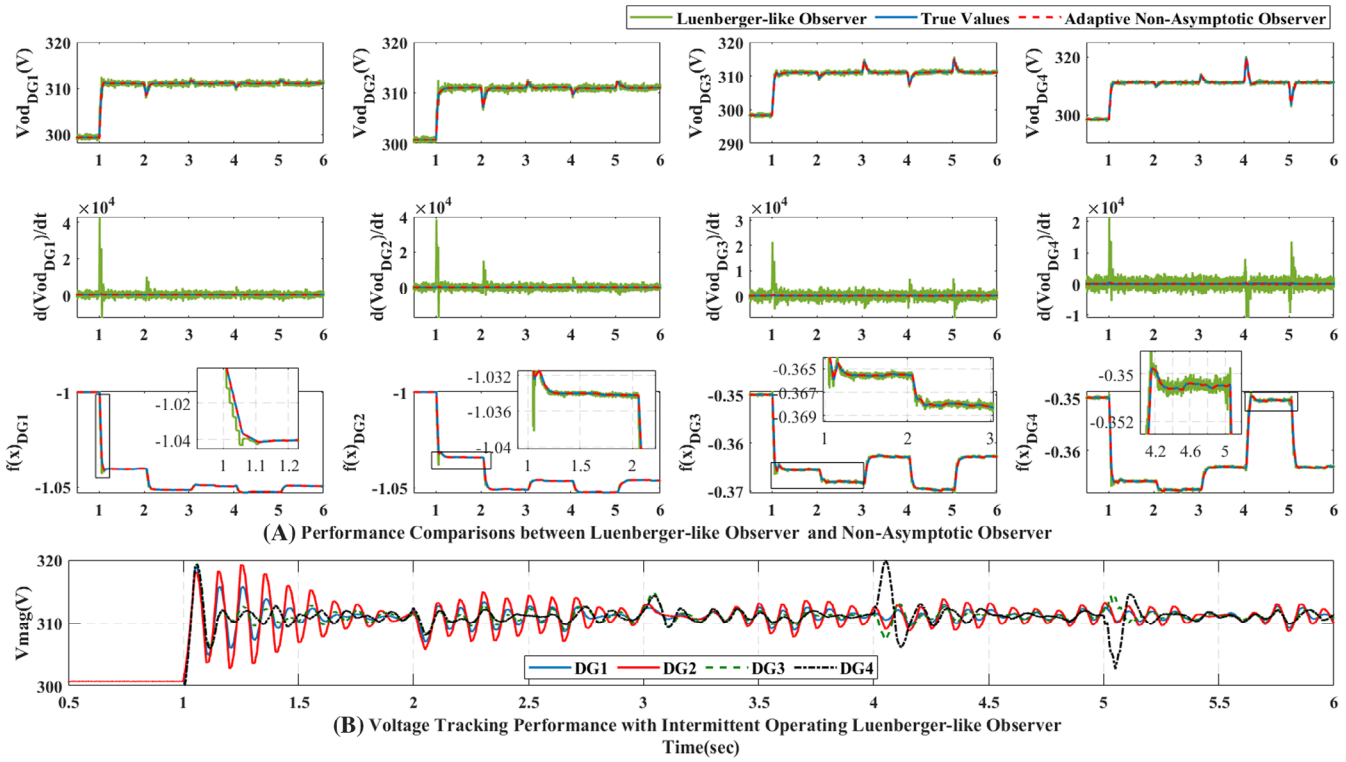

FIGURE 9 Voltage control performance with intermittent operating Luenberger-like observer [Colour figure can be viewed at wileyonlinelibrary.com]

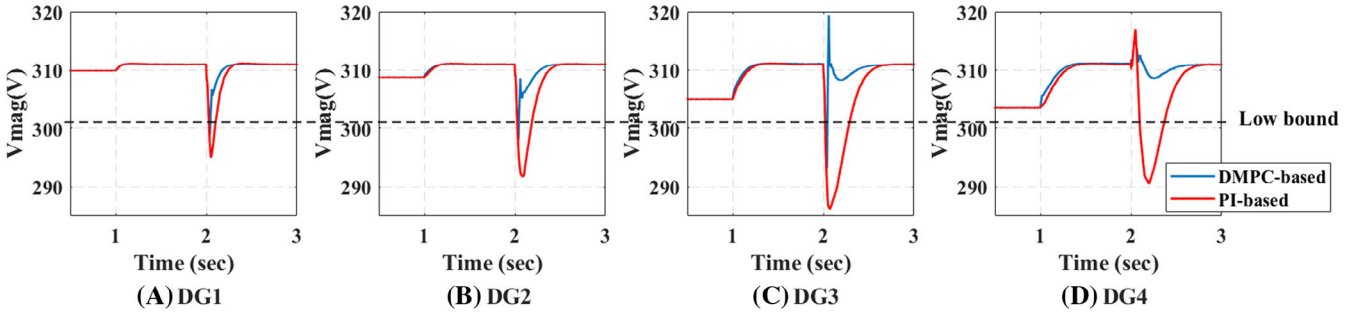

FIGURE 10 Voltage control performance under the extreme condition [Colour figure can be viewed at wileyonlinelibrary.com]

degrading control performance and at the same time higher computation and communication rates (increasing by 70.6% and 81.0% respectively as horizon decreases from 10 to 2).

4.1.4 | Scenario 4: Communication topology change

In Scenario 4, we consider communication interruptions which may occur in the distributed operation, and the physical and cyber events is shown in Figure 14. In the cyber layer, the communication change mimics the failure and recovery of cyber links. In practice, the recovery of communication links takes a finite period of time depending on the numbers of attacked nodes and broken communication links.[35] In this scenario, from 2 to 6 seconds, several failure and recovery events occur. The corresponding control performance is shown in Figure 15. The voltage tracking performance is maintained during the whole event, although DG4 does not always have the neighboring information over the time period 2 seconds $< t <$ 6 seconds. This is due to the prediction mechanism in the DMPC algorithm, under which DG4 can update

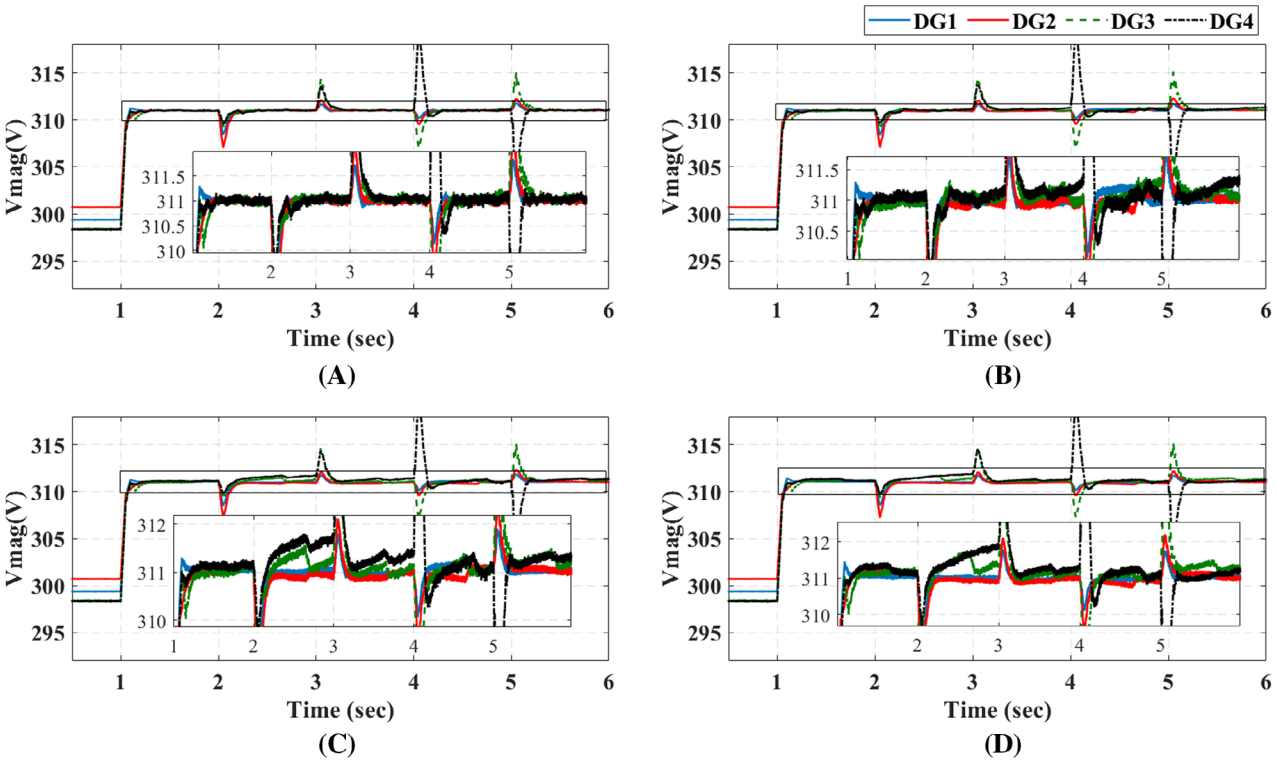

FIGURE 11 Event-triggered condition with fixed e_{com} ($e_{com} = 0.1$) but different thresholds e_{opt}: A, $e_{opt} = 0.05$; B, $e_{opt} = 0.1$; C, $e_{opt} = 0.15$; D, $e_{opt} = 0.2$ [Colour figure can be viewed at wileyonlinelibrary.com]

TABLE 3 Computation and communication reductions with fixed e_{com} ($e_{com} = 0.1$) but different thresholds e_{opt}

	e_{opt}	DG1	DG2	DG3	DG4	Average
Computation reduction	0.05	24%	24%	34%	34%	29%
	0.1	77%	80%	68%	66%	72.75%
	0.15	83%	84%	83%	81%	82.75%
	0.2	87%	84%	85%	83%	84.75%
Communication reduction	0.05	95%	89%	84%	84%	88%
	0.1	92%	86%	74%	69%	80.25%
	0.15	88%	77%	65%	64%	73.5%
	0.2	86%	78%	64%	65%	73.25%

the neighboring information according to the information received before the communication failure occurs. In other words, the prediction model in the event-triggered DMPC helps maintain the control performance in this extreme condition, which enhances the operational resilience. However, the PI-based control can only use the last received information before the communication failure, so it could lead to the tracking error if the system has not entered into the steady state at the time instant when the communication failure occurs. Due to that communication failure can be caused by many practical reasons such as denial of service, actual faults, it is reasonable that there exists load change during the communication failure, thus the proposed DMPC-based control will show better resilience in practice.

4.2 | Case 2: Modified IEEE-13 bus system

A real MG system is utilized to further test the effectiveness of the proposed method. The electrical and communication topology of the modified IEEE-13 bus test system[36] is shown in Figure 16, where there is a breaker

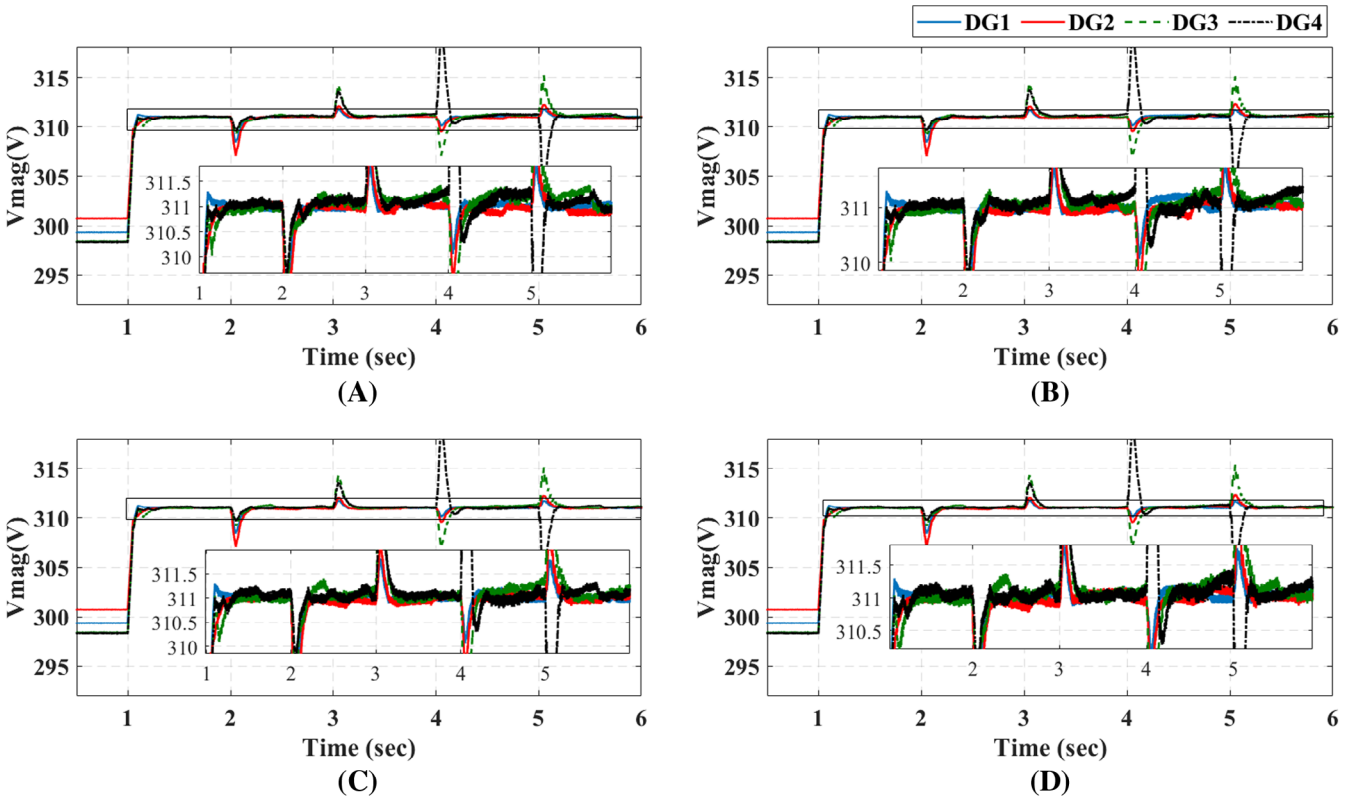

FIGURE 12 Event-triggered condition with fixed e_{opt} ($e_{opt} = 0.1$) but different thresholds e_{com}: A, $e_{com} = 0.05$; B, $e_{com} = 0.1$; C, $e_{com} = 0.15$; D, $e_{com} = 0.2$ [Colour figure can be viewed at wileyonlinelibrary.com]

	e_{com}	DG1	DG2	DG3	DG4	Average
Computation reduction	0.05	77%	79%	69%	71%	74%
	0.1	77%	80%	68%	66%	72.75%
	0.15	79%	80%	73%	64%	74%
	0.2	78%	75%	69%	71%	73.25%
Communication reduction	0.05	67%	42%	42%	41%	48%
	0.1	92%	86%	74%	69%	80.25%
	0.15	96%	91%	81%	80%	87%
	0.2	96%	93%	86%	88%	90.75%

TABLE 4 Computation and communication reductions with fixed e_{opt} ($e_{opt} = 0.1$) but different thresholds e_{com}

between node 671 and 692. The parameters of six DGs are the same as those shown in Table A1 (DG5 is the same as DG4, DG6 is the same as DG1). The controller parameters remain the same as well. Due to the fact that this subsection focuses on the scalability and especially the resilience against potential system reconfiguration. The event triggering thresholds are set to $e_{opt} = 0.1, e_{com} = 0.1$ by following a similar tuning process elaborated in Subsection 4.1.2.

4.2.1 | Scenario 1: Scalability test

In this scenario, the breaker between nodes 671 and 692 is always switched on, and the scalability of the proposed control is illustrated by load change and DG's plug-and-play scenario: loads at bus 645 and bus 675 are decreased and increased at $t = 2, 3$ seconds respectively; and DG4 is disconnected and reconnected at $t = 4$ seconds and $t = 5$ seconds, respectively.

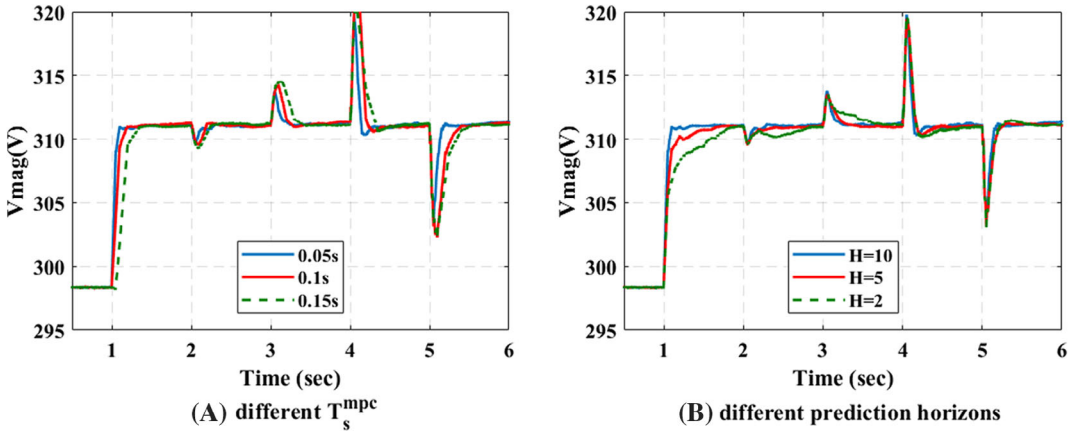

FIGURE 13 Effects of information update frequency and prediction horizon [Colour figure can be viewed at wileyonlinelibrary.com]

FIGURE 14 Physical and cyber events of the 4-DG MG system: value "1" represents that the communication channel between DG3 and DG4 is unavailable; the load change occurs at 2, 4, and 5 seconds, respectively [Colour figure can be viewed at wileyonlinelibrary.com]

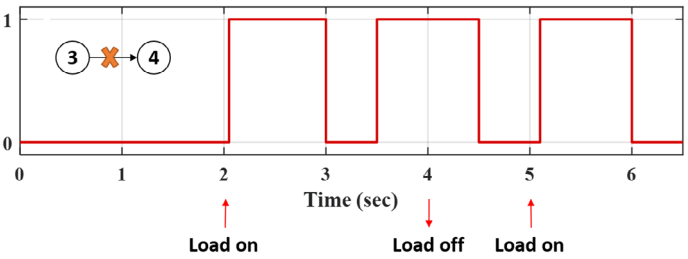

FIGURE 15 Voltage control performance with cyber and physical events [Colour figure can be viewed at wileyonlinelibrary.com]

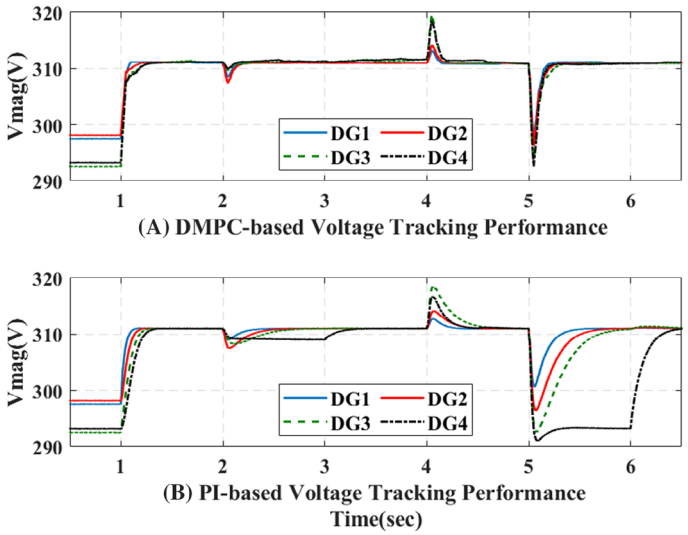

The voltage tracking performance is shown in Figure 17 and the average reductions of computation and communication are 57.42% and 88.48%.

4.2.2 | Scenario 2: Resilience illustration with system reconfiguration

To evaluate the resilience of the proposed voltage regulation method when the system reconfiguration occurs on both physical and cyber layers, we design the physical and cyber events (including breaker switched off and on) as shown in Figure 18. The corresponding control performance is shown in Figure 19. Although there are both physical and cyber events, similar to the Subsection 4.1.4, the voltage tracking performance is guaranteed by using event-triggered DMPC

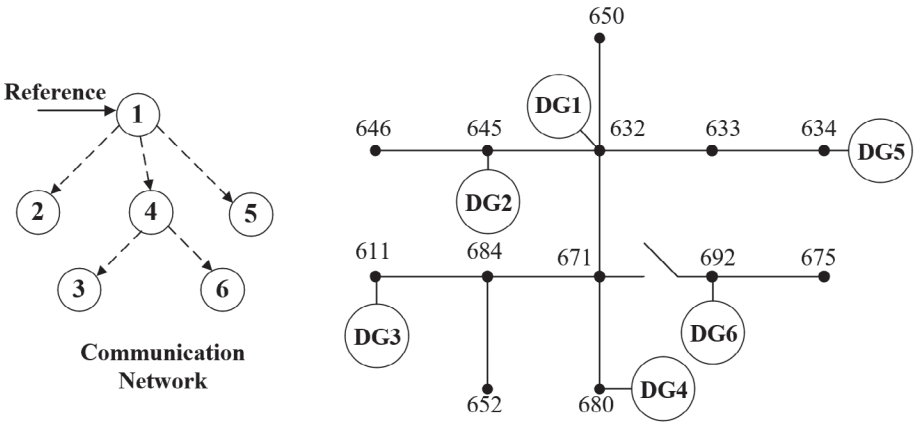

FIGURE 16 Diagram of modified IEEE-13 bus MG system

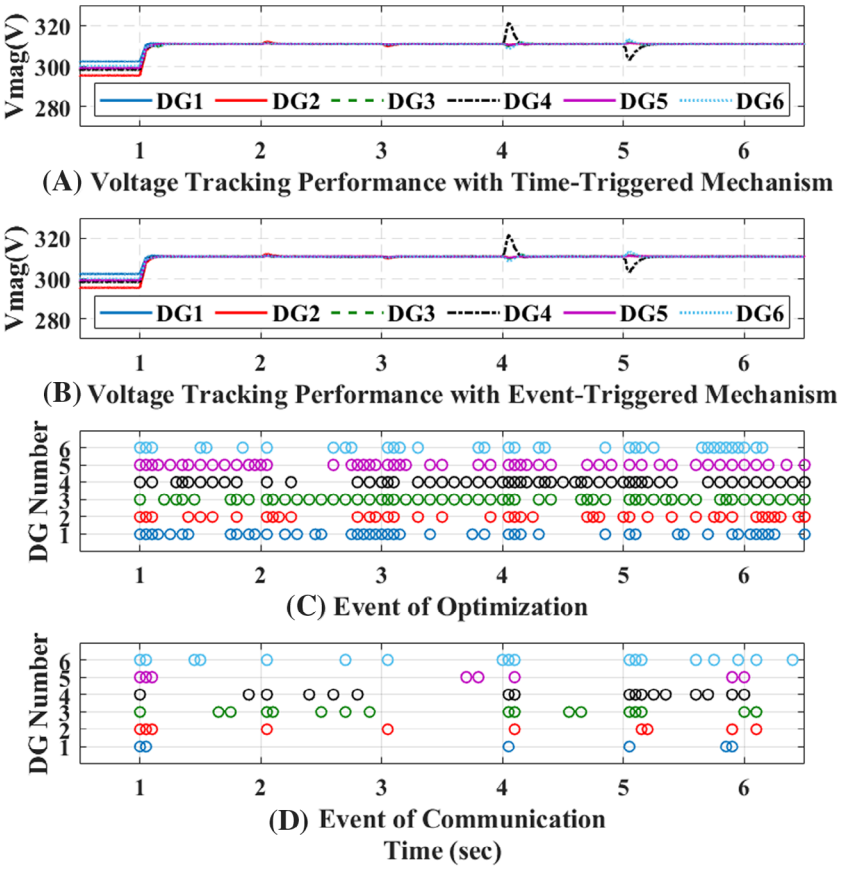

FIGURE 17 Voltage control performance of modified IEEE-13 bus MG system: A, voltage tracking performance with time-triggered mechanism; B, voltage tracking performance with event-triggered mechanism; C, event-triggered time of DMPC optimization; D, event-triggered time of neighboring communication [Colour figure can be viewed at wileyonlinelibrary.com]

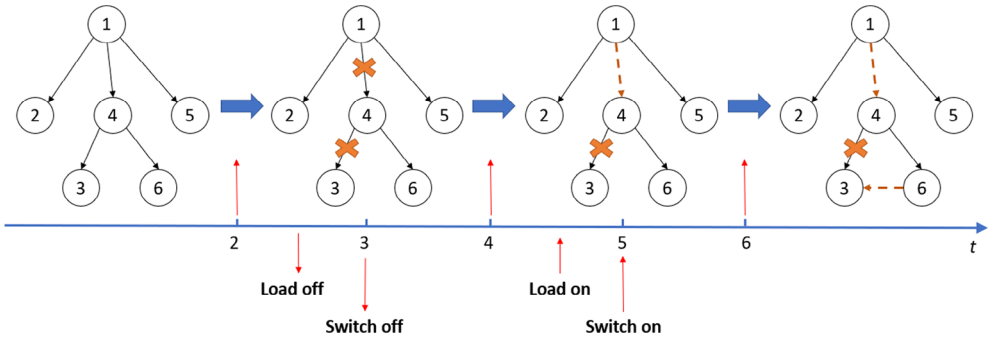

FIGURE 18 Physical and cyber events of modified IEEE-13 bus MG system [Colour figure can be viewed at wileyonlinelibrary.com]

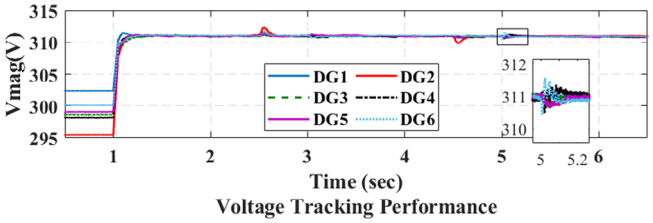

FIGURE 19 Voltage control performance with system reconfiguration in the modified IEEE-13 bus system [Colour figure can be viewed at wileyonlinelibrary.com]

method, and the average reductions of computation and communication are 63.94% and 88.03%. The oscillations at $t = 5$ seconds are incurred by the resynchronization after the break is switched on.

5 | CONCLUSION

This article proposes an event-triggered DMPC for secondary voltage control scheme in a cyber-physical coupled MG system, which explicitly considers the model nonlinearity and the system noise-resilience. In the control design, based on the event-triggered DMPC, two thresholds are designed to trigger the local DMPC computation and neighboring communications among DGs. To facilitate a cost-effective and noise-resilient control, an adaptive observer that features the nonasymptotic convergence characteristic is utilized, and this designed adaptive nonasymptotic observer can be coordinated with the DMPC voltage regulator in a timing sequence. Finally, the effectiveness of the proposed control method is verified on a 4-DG MG system and the modified IEEE-13 system.

ACKNOWLEDGMENT

This work was supported by EPSRC under Grant EP/T021780/1 and by ESRC under Grant ES/T000112/1.

ORCID

Pudong Ge https://orcid.org/0000-0002-9887-9572

REFERENCES

1. Ton DT, Smith MA. The U.S. department of energy's microgrid initiative. *Electr J*. 2012;25(8):84-94.
2. Olivares DE, Mehrizi-Sani A, Etemadi AH, et al. Trends in Microgrid Control. *IEEE Trans Smart Grid*. 2014;5(4):1905-1919.
3. Antoniadou-Plytaria KE, Kouveliotis-Lysikatos IN, Georgilakis PS, Hatziargyriou ND. Distributed and decentralized voltage control of smart distribution networks: models, methods and future research. *IEEE Trans Smart Grid*. 2017;8(6):2999-3008.
4. Wang C, Zhang T, Luo F, Li F, Liu Y. Impacts of cyber system on microgrid operational reliability. *IEEE Trans Smart Grid*. 2019;10(1):105-115.
5. Mehrizi-Sani A, Iravani R. Potential-function based control of a microgrid in islanded and grid-connected modes. *IEEE Trans Power Syst*. 2010;25(4):1883-1891.
6. Khayat Y, Shafiee Q, Heydari R, et al. On the secondary control architectures of ac microgrids: an overview. *IEEE Trans Pow Electron*. 2020;35(6):6482-6500.
7. Guerrero JM, Vasquez JC, Matas J, de Vicuna LG, Castilla M. Hierarchical control of droop-controlled ac and dc microgrids-a general approach toward standardization. *IEEE Trans Ind Electron*. 2011;58(1):158-172.
8. Zhang C, Xu Y, Dong Z, Ravishankar J. Three-stage robust inverter-based voltage/var control for distribution networks with high-level PV. *IEEE Trans Smart Grid*. 2019;10(1):782-793.
9. Díaz NL, Luna AC, Vasquez JC, Guerrero JM. Centralized control architecture for coordination of distributed renewable generation and energy storage in islanded AC microgrids. *IEEE Trans Pow Electron*. 2017;32(7):5202-5213.
10. Cady ST, Domínguez-García AD, Hadjicostis CNA. Distributed generation control architecture for Islanded AC microgrids. *IEEE Trans Control Syst Technol*. 2015;23(5):1717-1735.
11. Etemadi AH, Davison EJ, Iravani RA. Decentralized robust control strategy for multi-der microgrids-Part I: fundamental concepts. *IEEE Trans Pow Delivery*. 2012;27(4):1843-1853.
12. Bidram A, Davoudi A, Lewis FL, Guerrero JM. Distributed cooperative secondary control of microgrids using feedback linearization. *IEEE Trans Pow Syst*. 2013;28(3):3462-3470.
13. Riverso S, Sarzo F, Ferrari-Trecate G. Plug-and-play voltage and frequency control of islanded microgrids with meshed topology. *IEEE Trans Smart Grid*. 2015;6(3):1176-1184.
14. Wang Y, Nguyen TL, Xu Y, Li Z, Tran QT, Cyber-Physical Design CR. Implementation of distributed event-triggered secondary control in islanded microgrids. *IEEE Trans Ind Appl*. 2019;55(6):5631-5642.

15. Pilloni A, Pisano A, Usai E. Robust finite-time frequency and voltage restoration of inverter-based microgrids via sliding-mode cooperative control. *IEEE Trans Ind Electron*. 2018;65(1):907-917.
16. Abhinav S, Schizas ID, Lewis FL, Davoudi A. Distributed noise-resilient networked synchrony of active distribution systems. *IEEE Trans Smart Grid*. 2018;9(2):836-846.
17. Zhou Q, Shahidehpour M, Yan M, Wu X, Alabdulwahab A, Abusorrah A. Distributed secondary control for islanded microgrids with mobile emergency resources. *IEEE Trans Pow Syst*. 2020;35(2):1389-1399.
18. Anderson S, Hidalgo-Gonzalez P, Dobbe R, Tomlin CJ. Distributed model predictive control for autonomous droop-controlled inverter-based microgrids. Paper presented at: Proceedings of the 2019 IEEE 58th Conference on Decision and Control (CDC), Nice, France; 2019:6242-6248. https:/doi.org/10.1109/CDC40024.2019.9028938.
19. Zuo S, Davoudi A, Song Y, Lewis FL. Distributed finite-time voltage and frequency restoration in Islanded AC microgrids. *IEEE Trans Ind Electron*. 2016;63(10):5988-5997.
20. Ge P, Zhu Y, Green T, Teng F. Resilient Secondary Voltage Control of Islanded Microgrids: An ESKBF-Based Distributed Fast Terminal Sliding Mode Control Approach. *IEEE Transactions on Power Systems*. 2020;1-1. http://dx.doi.org/10.1109/tpwrs.2020.3012026.
21. Heemels WPMH, Johansson KH, Tabuada P. An introduction to event-triggered and self-triggered control. Paper presented at: Proceedings of the 2012 IEEE 51st IEEE Conference on Decision and Control (CDC); 2012:3270-3285; Maui, HI, IEEE. https://doi.org/10.1109/CDC.2012.6425820.
22. Lehmann D, Henriksson E, Johansson KH. Event-triggered model predictive control of discrete-time linear systems subject to disturbances. Paper presented at: Proceedings of the 2013 European Control Conference (ECC), Zurich; 2013:1156-1161. https:/doi.org/10.23919/ECC.2013.6669580.
23. Heemels WPMH, Teel AR, van de Wouw N, Nešić D. Networked control systems with communication constraints: tradeoffs between transmission intervals delays perform. *IEEE Trans Automat Control*. 2010;55(8):1781-1796.
24. Zhang B, Dou C, Yue D, Zhang Z, Zhang T. A Packet loss-dependent event-triggered cyber-physical cooperative control strategy for islanded microgrid. *IEEE Trans Cybern*. 2019;1-1. https://doi.org/10.1109/TCYB.2019.2954181.
25. Madoński R, Herman P. Survey on methods of increasing the efficiency of extended state disturbance observers. *ISA Trans*. 2015;56:18-27.
26. Ge P, Dou X, Quan X, et al. Extended-state-observer-based distributed robust secondary voltage and frequency control for an autonomous microgrid. *IEEE Trans Sustain Energy*. 2020;11(1):195-205.
27. Simpson-Porco JW, Shafiee Q, Dörfler F, Vasquez JC, Guerrero JM, Bullo F. Secondary frequency and voltage control of islanded microgrids via distributed averaging. *IEEE Trans Ind Electron*. 2015;62(11):7025-7038.
28. Floriduz A, Tucci M, Riverso S, Ferrari-Trecate G. Approximate Kron reduction methods for electrical networks with applications to plug-and-play control of AC islanded microgrids. *IEEE Trans Control Syst Technol*. 2019;27(6):2403-2416.
29. Dorfler F, Bullo F. Kron reduction of graphs with applications to electrical networks. *IEEE Trans Circ Syst I Reg Pap*. 2013;60(1):150-163.
30. Zhang H, Kim S, Sun Q, Zhou J. Distributed adaptive virtual impedance control for accurate reactive power sharing based on consensus control in microgrids. *IEEE Trans Smart Grid*. 2017;8(4):1749-1761.
31. Lewis FL, Qu Z, Davoudi A, Bidram A. Secondary control of microgrids based on distributed cooperative control of multi-agent systems. *IET Gener Trans Distrib*. 2013;7(8):822-831.
32. Li P, Boem F, Pin G, Parisini T. Distributed fault detection and isolation for interconnected systems: a non-asymptotic kernel-based approach. *IFAC-PapersOnLine*. 2017;50(1):1013-1018.
33. Pin G, Lovera M, Assalone A, Parisini T. Kernel-based non-asymptotic state estimation for linear continuous-time systems. Paper presented at: Proceedings of the 2013 American Control Conference, Washington, DC; 2013. 3123-3128. https:/doi.org/10.1109/ACC.2013.6580311.
34. Pin G, Chen B, Parisini T. Robust deadbeat continuous-time observer design based on modulation integrals. *Automatica*. 2019;107:95-102. https://linkinghub.elsevier.com/retrieve/pii/S0005109819302493.
35. Ding L, Han QL, Ning B, Yue D. Distributed resilient finite-time secondary control for heterogeneous battery energy storage systems under denial-of-service attacks. *IEEE Trans Ind Inform*. 2020;16(7):4909-4919. https://doi.org.10.1109/TII.2019.2955739.
36. Morstyn T, Hredzak B, Agelidis VG. Distributed cooperative control of microgrid storage. *IEEE Trans Pow Syst*. 2015;30(5):2780-2789.

How to cite this article: Ge P, Chen B, Teng F. Event-triggered distributed model predictive control for resilient voltage control of an islanded microgrid. *Int J Robust Nonlinear Control*. 2020;1–22. https://doi.org/10.1002/rnc.5238

APPENDIX

Dynamic models of DG inner loops

As shown in Figure 2, the instantaneous active and reactive powers are generated through a low-pass filter with the cutoff frequency $\omega_{ci} \ll \omega_i$:

$$\dot{P}_i = -\omega_{ci}P_i + \omega_{ci}(v_{odi}i_{odi} + v_{oqi}i_{oqi}), \tag{A1}$$

$$\dot{Q}_i = -\omega_{ci}Q_i + \omega_{ci}(v_{oqi}i_{odi} - v_{odi}i_{oqi}), \tag{A2}$$

where v_{odi}, v_{oqi} and i_{odi}, i_{oqi} are d-q voltage and current of the ith DG output, respectively. Apart from the droop control, the inner control loops (the voltage control loop and the current control loop) are modeled as:

$$\begin{cases} \dot{\phi}_{di} = v^*_{odi} - v_{odi} \\ \dot{\phi}_{qi} = v^*_{oqi} - v_{oqi} \\ i^*_{ldi} = F_i i_{odi} - \omega_b C_{fi} v_{oqi} + K_{PVi}(v^*_{odi} - v_{odi}) + K_{IVi}\phi_{di} \\ i^*_{lqi} = F_i i_{oqi} + \omega_b C_{fi} v_{odi} + K_{PVi}(v^*_{oqi} - v_{oqi}) + K_{IVi}\phi_{qi} \\ \dot{\gamma}_{di} = i^*_{ldi} - i_{ldi} \\ \dot{\gamma}_{qi} = i^*_{lqi} - i_{lqi} \\ \dot{v}^*_{ldi} = -\omega_b L_{fi} i_{lqi} + K_{PCi}(i^*_{ldi} - i_{ldi}) + K_{ICi}\gamma_{di} \\ \dot{v}^*_{lqi} = \omega_b L_{fi} i_{ldi} + K_{PCi}(i^*_{lqi} - i_{lqi}) + K_{ICi}\gamma_{qi} \end{cases}, \tag{A3}$$

where ϕ_{di}, ϕ_{qi}, and γ_{di}, γ_{qi} are auxiliary variables for the voltage controller and the current controller, respectively; K_{PVi}, K_{IVi} and K_{PCi}, K_{ICi} are P-I control parameters for the voltage controller and the current controller; ω_b represents the rated frequency of the MG; F_i is the parameter for d-q frame compensation. The dynamics of the LC filter and the output impedance also can be expressed as

$$\begin{cases} \dot{i}_{ldi} = -\frac{R_{fi}}{L_{fi}} i_{ldi} + \omega_i i_{lqi} + \frac{1}{L_{fi}} v_{idi} - \frac{1}{L_{fi}} v_{odi} \\ \dot{i}_{lqi} = -\frac{R_{fi}}{L_{fi}} i_{lqi} - \omega_i i_{ldi} + \frac{1}{L_{fi}} v_{iqi} - \frac{1}{L_{fi}} v_{oqi} \\ \dot{v}_{odi} = \omega_i v_{oqi} + \frac{1}{C_{fi}} i_{ldi} - \frac{1}{C_{fi}} i_{odi} \\ \dot{v}_{oqi} = -\omega_i v_{odi} + \frac{1}{C_{fi}} i_{lqi} - \frac{1}{C_{fi}} i_{oqi} \\ \dot{i}_{odi} = -\frac{R_{ci}}{L_{ci}} i_{odi} + \omega_i i_{oqi} + \frac{1}{L_{ci}} v_{odi} - \frac{1}{L_{ci}} v_{bdi} \\ \dot{i}_{oqi} = -\frac{R_{ci}}{L_{ci}} i_{oqi} - \omega_i i_{odi} + \frac{1}{L_{ci}} v_{oqi} - \frac{1}{L_{ci}} v_{bqi} \end{cases}, \tag{A4}$$

where i_{ldi}, i_{lqi} denote currents at the LC filter inductance; v_{bdi}, v_{bqi} denote the voltages at the connection bus in Figure 2.

Parameters

See Table A1.

TABLE A1 Parameters of the tested 4-bus MG system ($T_s^{mpc} = 0.05$ seconds, $T_s = 0.01$ seconds)

		DG1	DG2	DG3 and DG4
DGs	m_P	6.28×10^{-5}	9.42×10^{-5}	12.56×10^{-5}
	n_Q	0.5×10^{-3}	0.75×10^{-3}	1×10^{-3}
	R_f	0.1 Ω	0.1 Ω	0.1 Ω
	L_f	1.35 mH	1.35 mH	1.35 mH
	C_f	47μF	47μF	47 μF
	R_c	0.02 Ω	0.02 Ω	0.02 Ω
	L_c	2 mH	2 mH	2 mH
	K_{Pv}	0.05	0.05	0.1
	K_{Iv}	390	390	420
	K_{Pc}	10.5	10.5	15
	K_{Ic}	1.6×10^4	1.6×10^4	2×10^4
Lines	Line1	$R = 0.23\ \Omega,\ L = 318\ \mu H$		
	Line2	$R = 0.35\ \Omega,\ L = 1847\ \mu H$		
	Line3	$R = 0.23\ \Omega,\ L = 318\ \mu H$		
RL loads	Load1	$R = 2\ \Omega,\ L = 6.4mH$		
	Load2	$R = 4\ \Omega,\ L = 9.6mH$		
	Load3	$R = 6\ \Omega,\ L = 12.8mH$		
	Load4	$R = 6\ \Omega,\ L = 12.8mH$		
Control parameters	DMPC	$v_{ref} = 311(220\sqrt{2}), H = 10$		
	Thresholds	$e_{opt} = 0.1, e_{com} = 0.1$		
	Observer	$\varpi = 2.5, [\omega_0, \omega_1, \omega_2] = [1, 2, 3]$		